RADAR-BASED FALL DETECTION EXPLOITING TIME-FREQUENCY FEATURES

Luis Ramirez Rivera[†], *Eric Ulmer*[†], *Yimin D. Zhang*[‡], *Wenbing Tao*[§], *and Moeness G. Amin*[‡]

[†] Department of Electrical and Computer Engineering, Villanova University, Villanova, PA 19085, USA
[‡] Center for Advanced Communications, Villanova University, Villanova, PA 19085, USA
[§] School of Automation, Huazhong University of Science and Technology, Wuhan 430074, China

ABSTRACT

Falls of the elderly are a major public health concern. In this paper, we develop an effective fall detection algorithm for application in continuous-wave radar systems. The proposed algorithm exploits time-frequency characteristics of the radar Doppler signatures, and the motion events are classified using the joint statistics of three different features. The effectiveness of the proposed technique is verified through measurement data.

Index Terms— Assisted living, fall detection, time-frequency analysis, classification.

1. INTRODUCTION

Falls of the elderly are a major public health concern as they often result in disability [1]. Falls are the main cause of accidental death in the U.S. population over age 65 [2]. Immediate assistance after a fall can reduce complications of fall risk [3]. Therefore, it is very important to detect elderly falls in a timely and accurate manner so that immediate response and proper care can be rendered.

A number of techniques have been proposed to sense vital signs and motions for ambient assisted living [4, 5, 6]. These sensing techniques include those monitoring physiological signs (e.g., electrocardiography (ECG)) and accelerometers, camera and thermography, passive infrared sensors, and radio frequency identification (RFID) devices. Among those, ECG, accelerometers, and RFID require that devices be attached to human body, whereas laser vibrometer requires very accurate control or placement. Camera systems are sensitive to lighting conditions, may be obscured by walls and fabrics, and raise privacy concerns.

Radar is an excellent sensing modality due to its capability of detecting motions of humans. The general concept of radar-based system is to transmit an electromagnetic (EM) wave over a certain range of frequencies and analyze the radar return signals. Specifically, low-cost narrowband radar systems estimate the velocity of moving objects by measuring the frequency shift of the wave radiated or scattered by the object, known as the Doppler effects.

The human gait classification based on radar Doppler spectrograms was considered for different arm motion patterns in the context of urban sensing [7, 8]. Gait characterization using various machine learning algorithms shows effective and satisfied performance [9, 10]. In addition, a Hidden Markov model (HMM) based machine learning approach was applied for fall detection from a time-frequency sequence [11].

In this paper, we examine a different approach for radar-based fall detection that utilizes multiple features that are intrinsic to the time-frequency characteristics underlying the radar returns. By applying the short-time Fourier transform (STFT) to the raw data retrieved from the radar and analyzing the energy content of the signal, it is possible to identify potentially catastrophic events. These events are extracted from the data for a tri-characteristic analysis in order to classify the type of motion. The classification algorithm is examined between different motion patterns that respectively exhibit close and distinct Doppler signatures. For this purpose, we have selected falls, sitting and standing (S&S) motions, and bending over and standing up (B&S) motions for classification. We designed and performed experiments that would allow us to test the classification algorithm using the Villanova Radar Imaging Lab at the Center for Advanced Communications. With the data collected, we obtained quantifiable results to verify the reliability of the proposed classification algorithm.

2. SYSTEM AND SIGNAL MODEL

2.1. Signal Model

A continuous-wave (CW) radar is considered in this paper. Assume a sinusoidal signal, expressed as $s(t) = \exp(j2\pi f_c t)$, is transmitted from a transmitter, where f_c is the carrier frequency. Consider a point target which is located at a distance of R_0 from the radar, and moves with a velocity of $v(t)$ toward a direction which forms an angle of θ between the radar direction. As such, the distance between the radar and the target at time instant t is $R(t) = R_0 + \int_0^t v(u)\cos(\theta)du$, and the received radar signal is expressed as

$$x_a(t) = \rho \exp[j2\pi f_c(t - 2R(t)/c)], \tag{1}$$

where ρ is the target reflection coefficient and c is the velocity of EM wave propagation. The Doppler frequency corresponding to $x_a(t)$ is

$$f_D(t) = 2v(t)\cos(\theta)/\lambda, \tag{2}$$

where $\lambda = c/f_c$ is the wavelength.

For a rigid body target, such as a human body, the return signal is the integration over the target region, expressed as

$$x(t) = \int_{\Omega} x_a(t) da, \tag{3}$$

where Ω denotes the target region. As such, the Doppler signature is the superposition of each component Doppler frequencies. Torso or gait motions generally generate time-varying Doppler frequencies, and their exact signatures depend on the target shape and the motion patterns.

In our experimental studies, the radar data sets were collected in the Radar Imaging Lab at the Center for Advanced Communications, Villanova University. The experiment scene is shown in Fig. 1. An Agilent network analyzer was externally triggered with a time sampling rate of 1 kHz, and the carrier frequency is $f_c = 8$ GHz. Background subtraction was performed before processing the data. The periodic sampling results in discrete-time observations $x[k] = x(kT)$, where $T = 10^{-3}$ s is the sampling interval.

Fig. 1. Experiment scene.

2.2. Time-Frequency Analysis

By using joint time-frequency analysis methods, time-varying Doppler frequency can be captured at various instances of time. In this paper, we use the spectrogram, generated through the STFT, to perform the time-frequency analysis of the Doppler signature. The discrete-time STFT of signal $x(t)$ is defined as

$$X(t, f) = \sum_{m=-\infty}^{\infty} x(m) h(t - m) \exp(-j2\pi f m), \tag{4}$$

where $h(t)$ is the window function that trades off the time and frequency resolutions. We tested different Hamming window sizes and found that a window size of 255 is chosen for our processing. A larger window length may degrade the time resolution whereas as a smaller window length may compromise the frequency resolution, as seen in Fig. 2.

2.3. Power Burst Curve

After the proper spectrogram of the data is obtained, the algorithm determines exactly where important events have occurred in the data. We utilize a power burst curve (PBC) of the

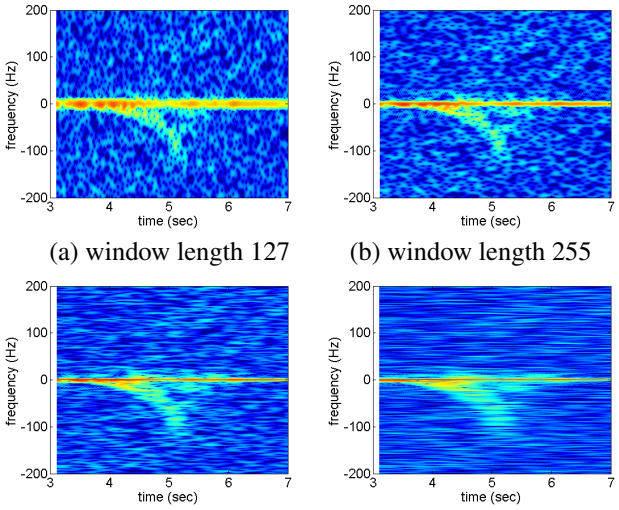

(a) window length 127 (b) window length 255

(c) window length 511 (d) window length 1023

Fig. 2. Spectrogram of fall generated with different window sizes.

data (which was referred to as the energy burst curve in [12] and [11]), which represents the summation of signal power within a specific frequency band between frequencies f_1 and f_2, expressed as

$$PBC(t) = \sum_{f=f_1}^{f_2} |X(f,t)|^2 + \sum_{f=-f_2}^{-f_1} |X(f,t)|^2. \tag{5}$$

We choose $f_1 = 70$ Hz and $f_2 = 100$ Hz to detect high-energy events, as catastrophic events, such as falls, typically have high Doppler energy content within this frequency band.

The PBC of the ambient noise can be considered to follow a Gaussian distribution, denoted as $\mathcal{N}(\mu_P, \sigma_P)$, where μ_P and σ_P respectively denote the mean and variance of the distribution. To keep the algorithm sensitive to human event whereas sufficiently separated from the noise floor, the following threshold is used for event detection:

$$\eta_P = \mu_P + 6\sqrt{\sigma_P}. \tag{6}$$

Therefore, an event is determined whenever the PBC exceeds this threshold, initiating the classification procedure as described in the following section. Fig. 3 shows one example of the PBC where a fall occurs.

3. CLASSIFICATION

Once an event is detected by thresholding the PBC, we construct a 4-second window of the spectrogram, centered around each of these points, to determine whether a fall has happened. The proposed technique consists of segmentation and morphological processing to obtain a clean binary time-frequency signature, which is then used to perform a tri-characteristic analysis that determines the type of motion represented in each window.

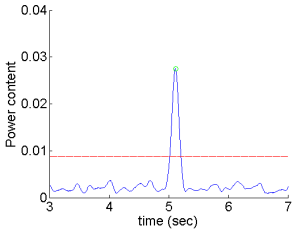

Fig. 3. An example of the PBC. The red line represents the detection threshold.

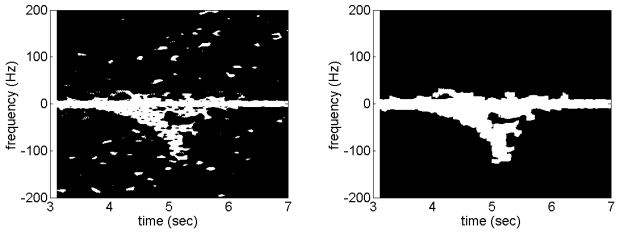

Fig. 4. Binary time-frequency signature obtained from the spectrogram.

3.1. Spectrogram Segmentation and Morphological Processing

To obtain a clean binary time-frequency signature of the interested activities for the classification, the following two important steps are executed on the spectrogram results: (a) image segmentation; and (b) morphological operator. In this work, the latter step includes image dilation and disconnected region removal.

The objective of image segmentation is to separate the Doppler signatures of human events from background noise. The segmentation is performed using gray-scale spectrogram images. In this case, thresholding is a commonly used image segmentation technique [13, 14]. The determination of an appropriate threshold value, which separates or segments a gray-level time-frequency representation into target events and background noise regions, is an important task of a thresholding algorithm. Because the presence of the Doppler signature is usually very weak around the extreme frequencies, which are used as an important feature in the sequel, it is important that the threshold is not too high to reject such weak signals, whereas it is not too low as well so that the entire time-frequency domain is cluttered.

The spectrogram may consist of weak components, particularly around the extreme frequencies, which may yield broken segments after spectrogram segmentation [15]. Morphological operation [16], specifically dilation, can bridge closely related broken segments together. On the other hand, the removal of disconnected regions will only keep the significant time-frequency region which represent the target activities. Note that the effect of dilation should be compensated with the known number of dilated pixels in the peak frequency determination.

Fig. 4 shows the binary time-frequency signature, corresponding to the spectrogram depicted in Fig. 2(b), respectively after segmentation and morphological operator. The threshold level used for segmentation is $\mu + 1.5\sqrt{\sigma}$, with μ and σ respectively denoting the mean and variance of the noise power in the spectrogram, which provides a good trade-off between weak signal preservation and noise rejection.

3.2. Feature Definition and Fusion

For motion classification and fall detection, the following three features are chosen: extreme frequency magnitude, extreme frequency ratio, and length of event.

3.2.1. Extreme Frequency Magnitude

The extreme frequency magnitude is determined by

$$F = \max(f_{+\max}, -f_{-\min}), \tag{7}$$

where $f_{+\max}$ and $f_{-\min}$, respectively, denote the maximum frequency in the positive frequency range and the minimum frequency in the negative frequency range. Critical falls often exhibit a significant amount of energy in frequencies of great magnitude when compared to other types of observed motions.

3.2.2. Extreme Frequency Ratio

The extreme frequency ratio is defined as

$$R = \max\left(\left|\frac{f_{+\max}}{f_{-\min}}\right|, \left|\frac{f_{-\min}}{f_{+\max}}\right|\right). \tag{8}$$

For extreme falls, there is only high energy content in either the positive or negative frequencies, resulting a high extreme frequency ratio. On the other hand, other types of motions, such as sitting and standing, often demonstrate high energy content in both the positive and negative frequency bands, corresponding to a low extreme frequency ratio.

3.2.3. Length of Event

This feature is the length of time, in milliseconds, between the start and the end of an event, i.e.,

$$L = t_{\text{extrm}} - t_{\text{begin}}, \tag{9}$$

where t_{extrm} denotes the time where the extreme frequency occurs, whereas t_{begin} denotes the corresponding beginning time the event has initiated. The beginning of an event is determined by the time when the magnitude of the frequency content of a signal passes a specific threshold. In general, there were significant distinctions in the time spans of the three critical motions that we were comparing.

3.2.4. Feature Extraction and Fusion

Assume that the three feature parameters, F, R, and L, follow the joint Gaussian distribution with probability density function (pdf) $\mathcal{N}(\boldsymbol{\mu}^{(q)}, \boldsymbol{\Sigma}^{(q)})$, where superscript $(\cdot)^{(q)}$ denotes the

class of events, i.e., $q \in \{\text{Fall}, \text{S\&S}, \text{B\&S}\}$. In addition, $\boldsymbol{\mu}^{(q)} = [\mu_R^{(q)}, \mu_F^{(q)}, \mu_L^{(q)}]^T$ denotes the mean vector obtained from the training data belong to class q, where $(\cdot)^T$ denote transpose, and $\boldsymbol{\Sigma}^{(q)}$ is the corresponding covariance matrix. Specifically, $\boldsymbol{\Sigma}^{(q)} = \text{diag}[\sigma_R^{(q)}, \sigma_F^{(q)}, \sigma_L^{(q)}]$ in case $F^{(q)}$, $R^{(q)}$, and $L^{(q)}$ are independently distributed, where $\text{diag}(\cdot)$ denotes forming a diagonal matrix from a vector.

Denote $\mathbf{y}_p = [F_p, R_p, L_p]^T$ as the feature set obtain from data set p to be classified. Then, the joint pdf of $\mathbf{y}_p$ with respect to class q is expressed as

$$f(\mathbf{y}_p^{(q)}) = \frac{1}{(\sqrt{2\pi})^3 \det(\boldsymbol{\Sigma}^{(q)})} \cdot \exp\left(-\frac{1}{2}(\mathbf{y}_p - \boldsymbol{\mu}^{(q)})^T (\boldsymbol{\Sigma}^{(q)})^{-1} (\mathbf{y}_m - \boldsymbol{\mu}^{(q)})\right), \tag{10}$$

where $\det(\cdot)$ denotes the determinant.

The logarithm of the exponent in the joint pdf can be used to determine the following Mahalanobis distance [17]

$$D^{(q)}(\mathbf{y}_p) = \left((\mathbf{y}_p - \boldsymbol{\mu}^q)^T (\boldsymbol{\Sigma}^{(q)})^{-1} (\mathbf{y}_p - \boldsymbol{\mu}^{(q)})\right)^{1/2}. \tag{11}$$

Observation vector $\mathbf{y}_p$ is classified to class q when

$$D^{(q)}(\mathbf{y}_p) < D^{(k)}(\mathbf{y}_p), \forall k \neq q. \tag{12}$$

4. EXPERIMENT RESULTS

4.1. Experiment Settings

We conducted experiments for 8 different motion patterns, with each experiment pattern repeated for 10 times (5 times each for 2 objects). The recording time for each experiment is 20 seconds. Every set of experiments contains a different type of motion, including forward falling, backward falling, sitting and standing, and bending over and standing up. We also split each motion pattern into two different variations, one demonstrating a standard type of motion whereas the other one demonstrating a high-energy form of that motion in order to study the impact of such variations on the classification performance. The typical spectrograms of the 8 motion patterns are shown in Fig. 5. The first 4 patterns are collectively considered as falls, whereas the last 4 patterns are collectively considered as non-falls. The main objective of this paper is the detection of falls.

4.2. Detection and Classification Results

Table 1 summarizes the resulting confusion matrix obtained from the proposed technique for the 80 experiments being conducted. We only classify them into fall and non-fall patterns. The results generally show a good classification performance. The false negative case was due to very weak return signal from the target. Note that any single feature alone was not able to provide comparable fall detection performance.

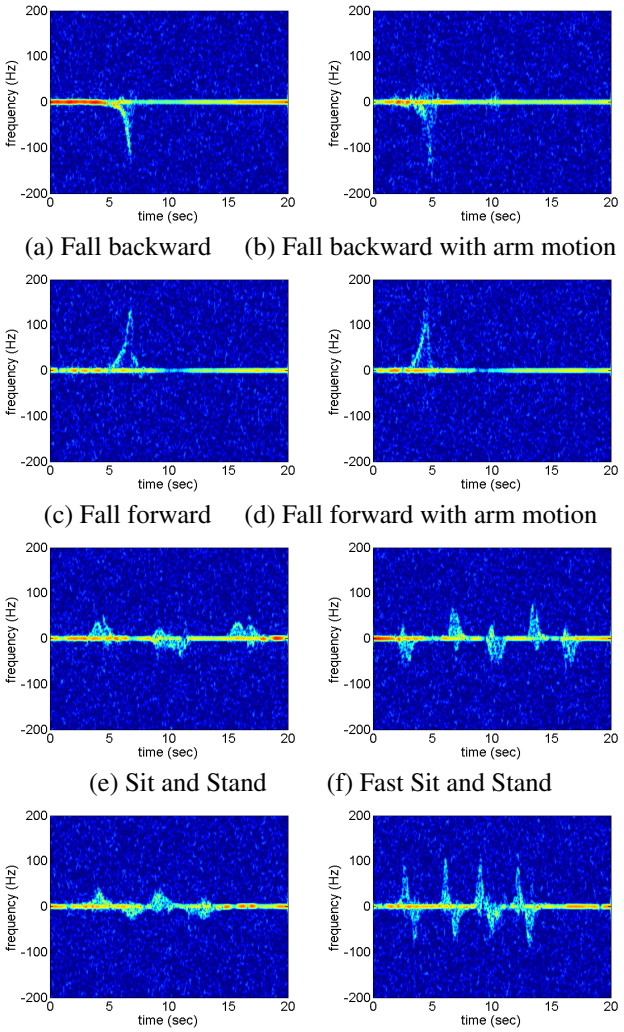

(a) Fall backward (b) Fall backward with arm motion

(c) Fall forward (d) Fall forward with arm motion

(e) Sit and Stand (f) Fast Sit and Stand

(g) Bend and stand (h) Fast bend and stand

Fig. 5. Spectrogram of typical motion patterns.

Table 1. Confusion matrix of the classification results

		Classified Class	
		Fall	Not Fall
Actual Class	Fall	39	1
	Not Fall	0	40

5. CONCLUSION

We have proposed an effective technique to process radar Doppler signatures for fall detection. The proposed technique treats the spectrogram as a gray-scale image, and image segmentation and morphological processing of spectrogram are performed before it is passed to perform feature analysis. Three parameters, namely, the extreme frequency magnitude, extreme frequency ratio, and the length of event, are used for the classification. The Mahalanobis distance between an unknown event under test and the known feature characteristics is used for classification.

REFERENCES

[1] S. Sadigh, A. Reimers, R. Andersson, and L. Laflamme, "Falls and fall related injuries among the elderly: a survey of residential-care facilities in a swedish municipality," *J. Community Health*, vol. 29, pp. 129–140, 2004.

[2] S. L. Murhy, "National vital statistics reports," tech. rep., National Center for Health Statistics, 2000.

[3] C. G. Moran, R. T. Wenn, M. Sikand, and A. M. Taylor, "Early mortality after hip fracture: is delay before surgery important," *J. Bone and Joint Surgery*, vol. 87, pp. 483–489, 2005.

[4] M. Chuah and F. Fu, "ECG anomaly detection via time series analysis," in *Proc. Int. Symp. Parallel and Distributed Proc. and Appli.*, pp. 121–140, Niagara Falls, Canada, Aug. 2007.

[5] A. Høst-Madsen, N. Petrochilos, O. Boric-Lubecke, V. M. Lubecke, B.-K. Park, and Q. Zhou, "Signal processing methods for Doppler radar heart rate monitoring," in D. Mandic, M. Golz, A. Kuh, D. Obradovic, and T. Tanaka (Eds.), *Signal Processing Techniques for Knowledge Extraction and Information Fusion,* Springer, pp. 121–140, 2008.

[6] O. Aardal, S.-E. Hamran, T. Berger, J. Hammerstad, and T. S. Lande, "Radar cross section of the human heartbeat and respiration in the 500mhz to 3ghz band," in *Proc. IEEE Radio and Wireless Symp.*, pp. 422–425, Phoenix, AZ, Jan. 2011.

[7] B. Mobasseri and M. G. Amin, "A time-frequency classifier for human gait recognition," in *Proc. SPIE,* vol. 7306, 2009.

[8] F. C. Tivive, A. Bouzerdoum, and M. G. Amin, "A human gait classificationmethod based on radar Doppler spectrograms," *EURASIP J. Adv. Sig. Proc.*, vol. 2010, pp. 1–12, 2010.

[9] Y. Kim and H. Ling, "Human activity classification based on micro-Doppler signatures using a support vector machine," *IEEE Trans. Geoscience and Remote Sensing*, vol. 47, pp. 1328–1337, 2009.

[10] L. Liu, M. Popescu, M. Skubic, M. Rantz, T. Yardibi, and P. Cuddihy, "Automatic fall detection based on Doppler radar motion signature," in *Proc. Int. Conf. Pervasive Computing Tech. for Healthcare*, 2011.

[11] M. Wu, X. Dai, Y. D. Zhang, B. Davidson, J. Zhang, and M. G. Amin, "Fall detection based on sequential modeling of radar signal time-frequency features," in *Proc. IEEE Int. Conf. Healthcare Informatics*, 2013.

[12] L. Liu, M. Popescu, M. Skubic, M. Rantz, T. Yardibi, and P. Cuddihy, "Automatic fall detection based on Doppler radar motion signature," in *Proc. IEEE Int. Conf. Pervasive Computing Tech. for Healthcare*, pp. 222–225, 2011.

[13] W. Tao, H. Jin, Y. Zhang, L. Liu, and D. Wang, "Image thresholding using graph cuts," *IEEE Trans. Systems, Man and Cybernetics, Part A*, vol. 38, pp. 1181–1195, Sep. 2008.

[14] W. Tao, H. Jin, and Y. Zhang, "Color image segmentation based on mean shift and graph cuts," *IEEE Trans. Systems, Man and Cybernetics, Part B*, vol. 37, pp. 1382–1389, Oct. 2007.

[15] P. Heidenreich, L. Cirillo, and A. Zoubir, "Morphological image processing for fm source detection and localization," *Signal Proc.*, vol. 89, pp. 1070–1080, 2009.

[16] R. Gonzalez and R. Woods, *Digital Image Processing*. Oxford, 2001.

[17] S. Theodoridis and K. Koutroumbas, *Pattern Recognition, third Ed.* Academic Press, 2006.